

H α detector system for the Helically Symmetric Experiment

S. P. Gerhardt, J. M. Canik, D. T. Anderson, and L. Owen

Citation: [Review of Scientific Instruments](#) **75**, 2981 (2004); doi: 10.1063/1.1784562

View online: <http://dx.doi.org/10.1063/1.1784562>

View Table of Contents: <http://scitation.aip.org/content/aip/journal/rsi/75/9?ver=pdfcov>

Published by the [AIP Publishing](#)

Articles you may be interested in

[Modeling, measurement, and 3-D equilibrium reconstruction of the bootstrap current in the Helically Symmetric Experiment](#)

Phys. Plasmas **21**, 092518 (2014); 10.1063/1.4895899

[Polarization separated Zeeman spectra from magnetic dipole transitions in highly charged argon in the large helical device](#)

Phys. Plasmas **14**, 042504 (2007); 10.1063/1.2714506

[Measurements and modeling of plasma flow damping in the Helically Symmetric eXperiment\)](#)

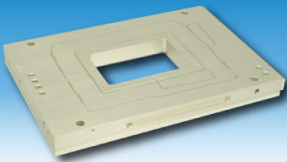
Phys. Plasmas **12**, 056116 (2005); 10.1063/1.1876293

[Polarization resolved H \$\alpha\$ spectra from the large helical device: Emission location, temperature, and inward flux of neutral hydrogen](#)

Phys. Plasmas **12**, 042501 (2005); 10.1063/1.1855323

[Calculations of neoclassical viscous damping on flux surfaces near magnetic islands in the Helically Symmetric Experiment](#)

Phys. Plasmas **12**, 012504 (2005); 10.1063/1.1825390



Nanopositioning Systems Micropositioning AFM & SPM Single molecule imaging

H_{α} detector system for the Helically Symmetric Experiment

S. P. Gerhardt,^{a)} J. M. Canik, and D. T. Anderson

HSX Plasma Laboratory, University of Wisconsin-Madison, Madison, Wisconsin 53706

L. Owen

Oak Ridge National Laboratory, Oak Ridge, Tennessee 37831

(Received 8 March 2004; accepted 19 May 2004; published 14 September 2004)

A system of absolutely calibrated H_{α} detectors for neutral hydrogen monitoring has been designed and implemented for the Helically Symmetric eXperiment. An array of detectors at fixed poloidal angle but many toroidal angles yields a measurement of the toroidal asymmetry in H_{α} emission and is used for monitoring hydrogen recycling. A multichord array at the toroidal angle of the gas puff allows an accurate determination of neutral gas penetration. Preliminary neutral gas modeling allows for the estimation of the density of atomic and molecular hydrogen from the H_{α} emission, which are used for particle transport and flow damping studies. © 2004 American Institute of Physics. [DOI: 10.1063/1.1784562]

I. INTRODUCTION

The Helically Symmetric eXperiment¹ (HSX) is the first of a new generation of stellarators² which exploit the concept of quasisymmetric magnetic fields.³ Conventional stellarators have large variations of $|B|$ in all directions on a magnetic surface, leading to large neoclassical flow damping and poorly confined particle orbits. By introducing a direction of symmetry to the configuration, the damping of flows in the symmetry direction is significantly reduced and particle orbits are closely tied to the magnetic surfaces.

A number of facets of the HSX program require a knowledge of the neutral atom density. Studies of plasma flow damping are in progress,⁴ and it is necessary to know the atomic hydrogen density to estimate the damping of the flows due to ion-neutral collisions. Particle transport studies have been initiated using both steady state⁵ and perturbative⁶ methods. These studies require knowledge of the particle source rate, which is directly coupled to the neutral density. Studies of superthermal electrons have been initiated, and it is necessary to know the neutral density to understand the impact of electron-neutral collisions on the energies that these electrons can attain.

A system of H_{α} detectors has been designed for neutral hydrogen monitoring on HSX, taking account of the specific features and needs of the device. The goals of the system included the ability to measure the relative contributions of wall recycling and gas puffing to the total hydrogen sources, as well as the penetration depth of neutral gas past the last closed magnetic surface. To meet these goals, two arrays of detectors were designed. One array was distributed around the machine toroidally at fixed poloidal angle, while another was at a fixed toroidal angle.

The layout of this article is as follows. Section II describes the goals of the system in more detail and how those

goals impacted the arrangement of the detectors around the machine. Section III describes the design of the detectors themselves. Section IV presents an example of the data collected by the system and illustrates the usefulness of the detector scheme. A brief description of the data analysis methods is given in Sec. V, followed by conclusions.

HSX is a moderately sized four field period stellarator at the University of Wisconsin-Madison. It has a major radius of 1.2 m and an average minor radius of 11 cm. The magnetic field is produced with a set of 48 nonplanar coils, and is currently operated at $B=0.5$ T with a maximum design specification of 1.2 T. Plasmas are formed and heated with a 28 GHz gyrotron, launching up to 200 kW of microwave radiation at the second cyclotron harmonic.

II. ARRANGEMENT OF THE DETECTORS ON HSX

In designing the arrangement of the system, a number of factors were considered. HSX is operated with only a single puff valve, whose wave form is preprogrammed to provide a specific density. This toroidally localized source, coupled to the large aspect ratio of the vessel, implies that a substantial toroidal asymmetry in the neutral density might be present if the gas puff dominates wall recycling in the total hydrogen source. For this reason, diagnosing any toroidal asymmetry in H_{α} emission was an important goal of the system. It was also considered important to determine the neutral gas penetration for estimation of the radial source profile. This implies the need for multiple detectors at the same toroidal angle but with chords having different impact parameters. Both of these needs have been satisfied with the system implemented on HSX.

The H_{α} detector system is composed of 15 detectors. The first array, called the poloidal array, is composed of nine detectors on the flange array at the tear-drop shaped cross section of the machine. This array is illustrated in Fig. 1; the magnetic field structure, both inside and outside the separatrix, is also illustrated for the base magnetic configuration of

^{a)}Present address: Princeton Plasma Physics Laboratory, Princeton, NJ 08543; electronic mail: sgerhard@pppl.gov

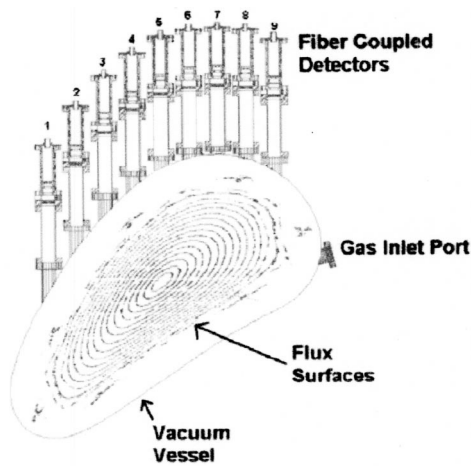


FIG. 1. Arrangement of detectors and gas puff at the poloidal array, as well as the vacuum vessel, magnetic surfaces, and edge island structures.

the machine. Note that the single gas puffer is located at the same toroidal angle, on a chord approximately orthogonal to sightlines of the detector. This arrangement allows for the determination of the neutral gas penetration. The chord numbers are given on the figure for future reference.

To monitor toroidal asymmetries, a set of seven detectors is located toroidally around the machine. This system is illustrated in Fig. 2. HSX is a four field period stellarator with the usual stellarator symmetry. It is composed of eight sections which can be copied onto each other after appropriate reflections and translations. Thus, the cross section and flange array illustrated in Fig. 1 exists once in each of the eight sections, and the central chord of these arrays was chosen as the location for the detector. In this arrangement, chord 5 of the poloidal array is also part of the toroidal array. With this arrangement, all toroidal array detectors view a section of the plasma with the same shape, and have the same chord lengths.

III. DESCRIPTION OF THE DETECTORS

The detectors were designed with certain HSX constraints in mind. A drawing of the detector, with all the relevant parts noted, is shown in Fig. 3. The HSX vacuum vessel is conditioned using helium glow discharge cleaning (GDC); this glow discharge can cause significant coating of windows which are placed too close to the vessel. Rather than use many complicated and expensive shutters, the vacuum window was placed at the end of a 3-in.-long and

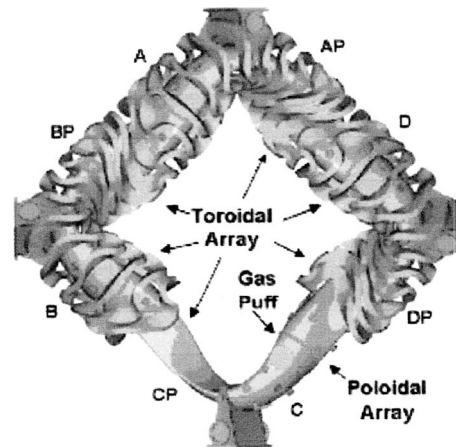


FIG. 2. Distribution of the toroidal array detectors around the stellarator, as well as the location of the gas puff and the nomenclature for labeling the half field periods.

0.75-in. inside diameter double nipple. This distance has proven sufficient to prevent the glow discharge from coating the windows. As a further complication, it can be seen from Fig. 1 that the amount of tubulation on the flanges welded to HSX differs significantly from chord to chord. To account for this fact, the light cone accepted by the detector is restricted so that it does not intersect the tube walls, even for the longest lengths of tubulation on the edge chords. This is illustrated by the acceptance cone in Fig. 3. With this design, it is unnecessary to introduce a calibration factor accounting for the different length of tubing on each chord.

The collection optics themselves are conventional. A quartz window (Insulator Seal 9722013) provides a metal sealed vacuum interface. The optics themselves are composed of a H_{α} filter (Coherent 42-5496) and a plano convex lens (Edmund Industrial Optics K45-305), which focus the light onto a large core diameter optical fiber (Thorlabs FT-1.0-UMT). This entire collection optics assembly is held in a black Delrin plastic housing.

The original design for the system called for the photo-detectors to be placed on the collection optics assembly at the torus itself. A prototype detector showed that the signal was contaminated by unexpected spikes. Testing revealed that these spikes were caused by x rays from superthermal electrons generated by the electron cyclotron heating (ECH) of the low density HSX plasmas. The fiber optics were then incorporated into the design to enable the detectors to be moved away from HSX and placed behind two layers of 0.125 in. lead shielding.

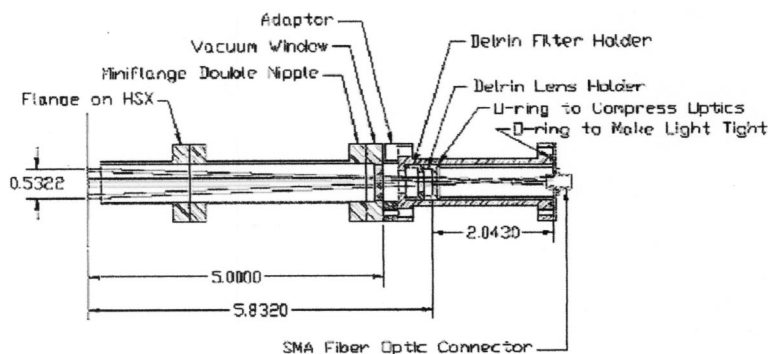


FIG. 3. Design of the collection optics of the H_{α} detector.

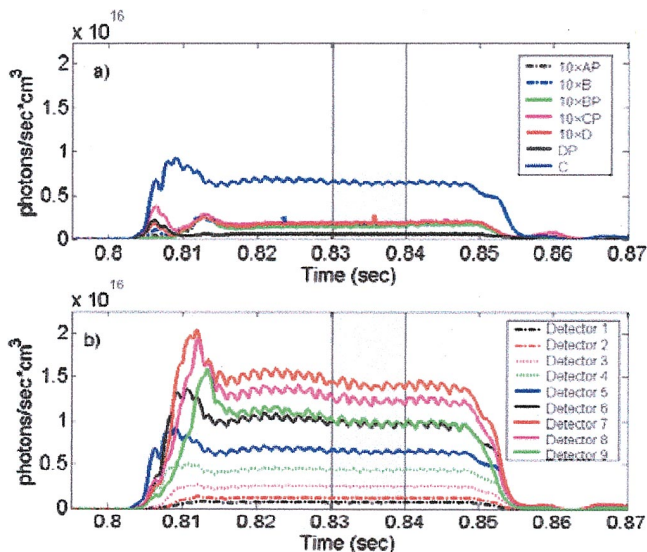


FIG. 4. (Color) Typical wave forms of the H α detector system from (a) the toroidal and (b) poloidal arrays.

The photodetector and amplifier are placed in a single aluminum box, one box per spatial channel. An SMA fiber coupler is mounted on the outside of the box, holding the fiber so that its light shines on the face of the detector. This detector consists of a photodiode and an op amp inside the same package (Advanced Photonix, SD-112-43-11-221), eliminating the need for an external transimpedance stage. The internal op amp is configured for a transimpedance of $10^8 \Omega$, and a bandwidth of 2 kHz. The signal from the detector is passed through a second gain stage; the gain in this stage has been set by the light levels at the various viewing locations. The toroidal array amplifiers generally require more gain than the poloidal array amplifiers, as the latter are located near the gas puff source of neutral gas. The signals from all 15 channels are recorded on the same digitizer at 10 kHz.

All detectors have been absolutely calibrated. The calibration was done using a 1 m spectrometer to accurately measure the transfer function of each H α filter and an absolutely calibrated integrating sphere light source to provide light of known spectral radiance.⁷ Apart from the second gain stage, the various detectors have similar calibration factors, determined mainly by the transmission of the H α filter.

IV. EXAMPLE OF DATA COLLECTED WITH THE SYSTEM

The H α wave forms a typical discharge are shown in Fig. 4. This stationary discharge had a line averaged density of $1 \times 10^{12} \text{ cm}^{-3}$, with launched ECH power of 25 kW between 0.800 and 0.850 s. The wave forms in the upper frame illustrate the signals from the toroidal array of detectors. Note that some of the signals have been multiplied by 10 so that they are visible on the same graph. The toroidal asymmetry due to the puff in field period C is readily apparent. The poloidal array signals are shown in the bottom frame. In general, those detectors near the puffer (chords 7–9) display larger signals than those farther away (chords 1–3), even though the path lengths are comparable. The signal on the

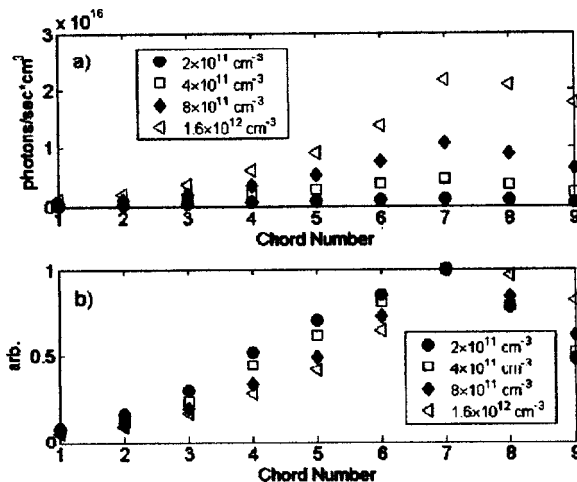


FIG. 5. (a) Profile of the H α emissivity at the poloidal array for different densities and (b) the same data normalized so that each profile has a maximum of one (bottom).

central chord (chord 5) is the first to rise, indicating the initial plasma forms on the magnetic axis where the electron cyclotron heating resonance is located.

Profiles of the line averaged emission for the poloidal array are shown in Fig. 5, for four different densities. The time window selected for these plots corresponds to the shaded areas in Fig. 4. In the top frame, the emission is plotted. In the bottom frame, each profile has been normalized so that the maximum value is one, enabling them to be easily compared. As the density rises, the relative and actual emission on chords near the puffer rises, reflecting the increased gas puff necessary to achieve that density. On the other hand, the emission away from the puffer decreases relative to the maximum, as shown in the lower part of the figure. This is caused by the improved screening of molecular hydrogen by the higher density plasmas. Room temperature molecular hydrogen has a mean free path of 2–5 cm in HSX, varying inversely with density. Hydrogen atoms with energies of 2–5 eV (the Franck–Condon energy) have mean free paths of ~ 0.5 m, compared to a minor radius of 0.1 m. Hence, atomic hydrogen is not screened in the radial direction, although there is substantial decay in the toroidal direction.

An example of how the toroidal array is used to determine the relative contributions to hydrogen fueling of wall recycling and gas puffing is presented in Fig. 6. We have selected a discharge immediately following a machine vent. The vessel walls have not been conditioned sufficiently to achieve density control in this discharge; the residual gas analyzer indicates that after a machine vent, significant amounts of water reside on the vessel walls until the proper conditioning has been performed. This conditioning process typically requires 10–30 full power discharges following helium GDC. The top frame shows the density rising until it reaches the cutoff for the second harmonic ECH, at which point the microwave absorption falls to near zero as evidenced by microwave absorption measurements.⁸ The gas puff wave form is also shown, indicating the decreasing rate of gas puff fueling throughout the discharge. The bottom

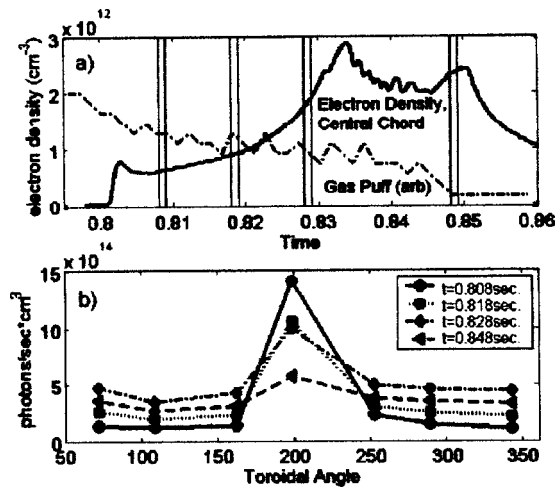


FIG. 6. (a) The density evolution (solid) and gas puff (--) of a discharge with a poorly conditioned vacuum vessel, and (b) the toroidal asymmetry in H_{α} emission at different times in the discharge. The times for the profiles correspond to the shaded areas of the time trace.

frame shows the toroidal array signals during the four windows indicated on the density trace. For the early window, a strong toroidal asymmetry is present with the peak at the location of the gas puff. As the discharge progresses and gas evolves off of the wall, the peaking at the gas puff location decreases. At the end of the discharge, the toroidal asymmetry has nearly completely disappeared. Hence, this system can provide the information for a determination of the contribution of recycling compared to gas puffing in the overall fueling.

V. INTERPRETATION OF THE DATA

Three-dimensional (3D) modeling is needed to deduce local neutral densities from the chordal H_{α} emission. There are two main reasons for this requirement. The signal contains contributions from both atomic hydrogen and the dissociation of molecular hydrogen, and hence is proportional to the densities of both neutral species. The H_{α} emission is fully three dimensional. Extracting the local 3D emissivity from the chordal data is a poorly posed inversion problem.

To resolve these problems, the 3D neutral gas code DEGAS⁹ has been implemented at HSX. This code requires specification of the sources of neutral gas as well as the plasma density and temperature profiles. The three-dimensional geometry of HSX is specified in the computational grid. Given this information, the code determines the distribution of neutrals due to the sources. It can then predict the line integrated H_{α} emission along chords specified by the user, allowing a straightforward comparison between the modeling and the experiment.

A preliminary comparison between the predicted and measured H_{α} chordal emission at the poloidal array is shown in Fig. 7. The figure illustrates the excellent agreement for all

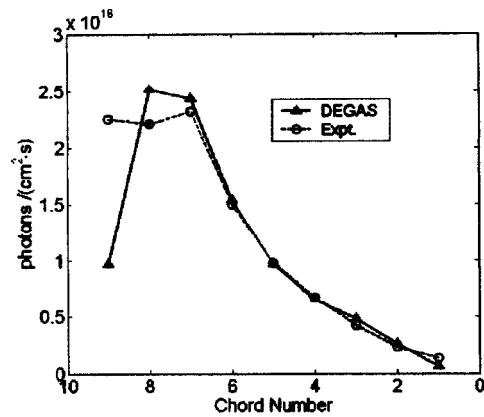


FIG. 7. Profile of the H_{α} emissivity at the poloidal array, compared to calculation with the neutral gas code DEGAS.

chords except the one nearest the puffer, where there is considerable uncertainty in the local plasma parameters on the open field lines. In the modeling a localized neutral gas source at the location of the puff is used in addition to modeled recycling; the electron density profile in the modeling is provided by inverted multi-chord interferometry.⁶ The DEGAS output has been scaled so that the prediction for chord 5 matches the measurement. The agreement between measured and predicted chordal data for the toroidal array is comparable to the poloidal array data presented here. The details of the three-dimensional neutral gas calculation, as well as more detailed comparisons between the modeling and experiment, will be presented in a future publication.

ACKNOWLEDGMENTS

The authors would like to thank Anthony Piccione for laying out the printed circuit board for the electronics, Mike Frankowski for the construction of the calibration apparatus, and Joe Talmadge for helpful discussions. This work was funded by the United States Department of Energy under Grant No. DE-FG02-93ER54222.

- ¹F. S. B. Anderson, A. F. Almagri, D. T. Anderson, P. G. Mathews, J. N. Talmadge, and J. L. Shohet, *Fusion Technol.* **27**, 273 (1995).
- ²A. H. Boozer, *Phys. Plasmas* **5**, 1647 (1998).
- ³J. Nührenberg and R. Zille, *Phys. Lett. A* **129**, 113 (1988).
- ⁴S. P. Gerhardt, D. T. Anderson, J. M. Canik, and J. N. Talmadge, *Proceedings of the 14th Stellarator Workshop*, Greifswald, Germany, September 2003 (unpublished).
- ⁵J. Canik, D. T. Anderson, S. P. Gerhardt, and J. N. Talmadge, in Ref. 4.
- ⁶C. Deng, D. L. Brower, W. X. Ding, A. F. Almagri, D. T. Anderson, F. S. B. Anderson, S. P. Gerhardt, P. Probert, and J. N. Talmadge, *Rev. Sci. Instrum.* **74**, 1625 (2003).
- ⁷Optronics Laboratory Series 455 Integrating Sphere Calibration Standard.
- ⁸K. M. Likin, J. N. Talmadge, A. F. Almagri, D. T. Anderson, F. S. B. Anderson, C. Deng, S. P. Gerhardt, and K. Zhai, 15th Topical Conference on Radio Frequency Power in Plasmas, Moran, WY, May 2003 (unpublished).
- ⁹D. B. Heifetz, D. Post, M. Petravac, J. Weisheit, and G. Bateman, *J. Comput. Phys.* **46**, 309 (1982).